Quantum soliton evaporation

Leone Di Mauro Villari,[1,2] Daniele Faccio,[1,3] Fabio Biancalana,[1] and Claudio Conti[2,4]
[1]*Institute of Photonics and Quantum Sciences, School of Engineering and Physical Sciences, Heriot-Watt University, Edinburgh EH14 4AS, United Kingdom*
[2]*Institute for Complex Systems, National Research Council (ISC-CNR), Via dei Taurini 19, 00185 Rome, Italy*
[3]*School of Physics and Astronomy, Kelvin Building, University of Glasgow, Glasgow G12 8QQ, United Kingdom*
[4]*Department of Physics, University Sapienza, Piazzale Aldo Moro 5, 00185 Rome, Italy*

(Received 26 October 2017; published 31 October 2018)

Quantum evaporation may occur in a variety of systems such as superfluids, Bose-Einstein condensates, and gravitational black holes (Hawking radiation). However, to date all predictions are based on semiclassical models, e.g., the Einstein equations and classical space-time metric for a black hole and only the fluctuations are quantized. Here we use a fully quantized dynamical equation, the quantum nonlinear Schrödinger equation, to study the evolution of quantum solitons. As a result of quantum fluctuations in the center-of-mass position, the expectation value of the quantum soliton width increases and concomitantly evaporates through the emission of frequency-entangled photon pairs. The frequency of this emission decreases as the soliton evaporates due to the soliton spreading. In the final phase, the soliton mean field collapses irreversibly into a state with zero mean amplitude. These results may provide insight to quantum evaporation in other systems where a full quantum description is still to be developed and highlights that even classically stable systems may also be subject to quantum evaporation.

DOI: 10.1103/PhysRevA.98.043859

I. INTRODUCTION

Quantum evaporation is a universal process through which a system loses energy by interaction with the environment as a result of the quantum nature of the system itself. One example is the quantum evaporation of superfluids whereby energy is lost through the emission of phonons [1] or rotons [2] into the normal component of the fluid. Quantum evaporation occurs also in bright [3] and dark [4,5] solitons propagation in the interaction with a quantum reservoir. Recent experiments have provided direct evidence of a quantum evaporation in Bose-Einstein condensates (BECs) in the presence of a transonic flow [6,7]. The most famous example, however, is the evaporation of gravitational black holes [8]. These systems share the same shortcoming in that they are described by a semiclassical model: a completely quantum description in which both the system and the interacting waves are fully quantized is lacking. For example, in the case of black hole evaporation the black hole is described by a classical space-time metric and the evolution follows from the Einstein equations. Only the vacuum fluctuations are quantized, as a result of which emission of particles and evaporation ensues. A model in which the black hole is also quantized (in the sense that the governing dynamical equations are quantized) is still to be found and given the difficulties encountered, the necessity for such a theory is under discussion (see, e.g., Refs. [9,10]). Here we provide evidence that a fully quantized model for quantum evaporation may be developed within the context of optical soliton evolution.

Solitons are localized analytical solutions of integrable nonlinear partial differential equations, such as the Korteweg-De Vries equation or the nonlinear Schrödinger equation (NLSE) [11,12]. As such, solitons occur in many different contexts, including light [13,14], ultracold gases [15], sound and water waves [16], and even in the brain synapses or in DNA dynamics [17–19]. It is possible to write a fully quantized version of the NLSE (QNLSE) and this was used to first study the quantum effects of pulse propagation in nonlinear fibers [20,21] and then to identify the existence of bound-state solutions from which it is possible to construct quantum soliton states [22,23]. Tightly related to the QNLSE, the generic quantum anharmonic oscillator equation predicts a phase diffusion effect due to random fluctuations in the photon or occupation number. This is followed by collapse of the quantum wave-function expectation value as seen in the average expectation that goes to zero, counterbalanced by an increase in the fluctuations around the mean zero value [24]. Further evolution then leads to periodic revivals of the initial soliton coherent state and the formation of Schrödinger cat states, a direct result of the quantization of the bound states [24,25]. This behavior was theoretically predicted to occur in quantum solitons, with a periodic collapse and revival of the wave-function amplitude that occurs over distances of the order of 10^7 km (or much smaller distances for the first collapse) [26]. These predictions were extended to the case of Bose-Einstein condensates (BECs) [27] and the periodic collapse and revival of the matter wave function was experimentally observed in a three-dimensional lattice [28]. All predictions mentioned above do not take into account fluctuations in the quantum soliton center of mass (COM) position.

A further key finding is that quantum solitons also undergo random fluctuations in COM position [23,29]. This effectively leads to suppression of the revivals: the quantum soliton is characterized by a single collapse [30] that is reminiscent of

 ©2018 American Physical Society

the same behavior of the quantum anharmonic oscillator in the presence of dissipation [31]. An intriguing semiclassical analog of the quantum soliton COM fluctuations due to interaction with the vacuum can be found in the Brownian motion of a matter wave soliton in the presence of a thermal cloud of atoms [32].

II. QUANTUM EVAPORATION

In the following we investigate different quantum soliton propagation regimes and show that the soliton loses energy through the emission of frequency-entangled photon pairs at a characteristic wave vector and frequency. We will refer to this as quantum evaporation.

We use the second quantized form of the NLSE [22,23,29]. By adopting the units in [22,23,29], denoted hereafter as the quantum soliton units, the quantum NLSE (QNLSE) reads

$$i\hat{\phi}_\tau(\xi,\tau)+\hat{\phi}_{\xi\xi}(\xi,\tau)+2\kappa\hat{\phi}^\dagger(\xi,\tau)\hat{\phi}(\xi,\tau)\hat{\phi}(\xi,\tau)=0, \quad (1)$$

where τ and ξ are the propagation and transverse coordinate, respectively, $\hat{\phi}$ the quantized scaled electromagnetic field in a one-dimensional nonlinear medium and $\kappa>0$ measures the strength of the self-focusing nonlinearity. The Bethe ansatz and quantum inverse scattering method [23,33] lead to the fundamental soliton solution as a superposition of the system's eigenstates $|n,p\rangle$ with Gaussian weights $g_n(p)$ [23], where n and p are photon number and momentum of each state.

$$|\psi_s,\tau\rangle=a_0|0\rangle+\sum_{n=1}^{\infty}a_n\int dp\, g_n(p)e^{-iE_{n,p}\tau}|n,p\rangle. \quad (2)$$

Here Δp is the variance of the distribution $g_n(p)$, and the classical soliton corresponds to $\Delta p=0$. In the most general case, the quantum expectation value of the field operator $\hat{\phi}(\xi)$ with respect to the state $|\psi\rangle$ is given by the average of a set of classical soliton solutions with different group and phase velocities. The quantum soliton therefore displays phase diffusion and wave-packet spreading [23].

In dimensional units, and with reference to an optical fiber [13], we have the following expression for the soliton width (calculated as the standard deviation) during propagation along the z axis:

$$\langle\Delta t^2\rangle\approx t_0^2+\frac{\hbar^2\omega_0^2}{\Delta t_0^2\mathcal{E}^2}\beta_2^2z^2, \quad (3)$$

where $\beta_2<0$ is the second-order dispersion coefficient [13], ω_0 is the optical angular frequency, $\mathcal{E}$ is the soliton energy, and t_0 is the initial soliton width. The soliton width relates to the Gaussian distribution variance Δp, that plays an important role in the quantum properties of the soliton dynamics, with the following formula

$$\Delta p=\frac{\hbar\omega_0\beta_1}{t_0\mathcal{E}}, \quad (4)$$

where β_1 is the inverse group velocity. Equation (3) gives the spreading of the soliton width during propagation. For $\hbar\to0$ the z-dependent part of Eq. (3) goes to zero, and this corresponds to the fact that the classical soliton is stable and does not disperse in the absence of quantum effects. The same occurs when the number of quanta $n_0=\mathcal{E}/\hbar\omega_0$ in the soliton goes to infinity. In contrast, in the quantum regime the soliton exhibits collapse [26,30].

We next show that the quantum collapse is accompanied by emission of radiation in the form of spectral sidebands. Using the full quantum theory we obtain the spectrum $S(k_\xi,\tau)$ of the field operator $\hat{\phi}(\xi)$ as the square modulus of the expectation value of the annihilation operator on the soliton state $|\psi_s\rangle$. To accomplish this calculation we use a second-order asymptotic expansion (details in Appendix B). We may calculate the spectrum $S(k_\xi,\tau)$ of the field operator $\hat{\phi}(\xi)$ as $|\langle\hat{a}^\dagger\hat{a}\rangle|^2$. We consider instead the quantity $|\langle a\rangle|^2$ that corresponds to the macroscopic wave function for a BEC. Use of this second quantity leads to an analytically simple formula that is a good approximation to the spectrum for quantum states that remain close to a coherent state. We verified numerically that these two choices of spectrum do not differ markedly in our simulations. This may be ascribed to the specific features of quantum solitons, which seem to preserve a nearly coherent state description. This is consistent with the fact that the coherent states are maximally stable with respect to interaction with a reservoir [34]. We therefore calculate the spectrum in terms of the momentum cutoff $\bar{p}=\omega_0/c$, due to the narrow band of the field around ω_0, as originally outlined in Ref. [35]. This quantity represents the quantum counterpart of the modulus squared of the Fourier transform of the classical field (expectation of the annihilation operator $\hat{a}$), which is in turn the Fourier transform of the field operator $\hat{\phi}$ [23]:

$$S(k_\xi,\tau)=|\langle a\rangle|^2\approx\frac{1}{2\bar{p}^2n_0^2\tau^2}\operatorname{sech}^2\left(\frac{\pi k_\xi}{\kappa n_0}\right) e^{-\frac{2\bar{p}^2}{\Delta p^2}-\frac{2k_\xi^2}{n_0^2\Delta p^2}}\left[\cosh\left(\frac{2}{\Delta p^2}\frac{k_\xi}{n_0}\bar{p}\right)+\cos\left(\bar{p}k_\xi\tau\right)\right]. \quad (5)$$

The idea behind this calculation represents a further extension of the concepts and techniques developed in Refs. [22,23,25].

Figure 1 shows the calculated spectrum for various soliton powers and reveal that, in addition to the dominant low-frequency classical spectrum represented by the central peak in Fig. 1, one finds a quantum contribution peaked at a characteristic frequency $k_\xi^{(e)}$. The lateral spectral tails in correspond to the spontaneous emission from the soliton and the resulting evaporation. From Eq. (5) we may compute the relation between the emission peak wave number $k_\xi^{(e)}$ and Δp. For quantum solitons with $n_0\gg n_0\kappa\gg1$, and considering the emission on the timescale of the soliton collapse, i.e., $\tau_1=1/(n_0\kappa\Delta p)$ [30], we have from Eq. (5)

$$S(k_\xi,\tau_1)\approx\frac{2}{n_0^2\tau^2}\operatorname{sech}^2\left(\frac{\pi k_\xi}{n_0\kappa}\right)\left[1+\cos\left(\frac{\bar{p}k_\xi}{n_0\kappa\Delta p}\right)\right]. \quad (6)$$

The corresponding peak emission then occurs at

$$k_\xi^{(e)}=\pi n_0\kappa\frac{\Delta p}{\bar{p}}. \quad (7)$$

Equation (7) shows that there is a linear dependence of the emission peak with Δp.

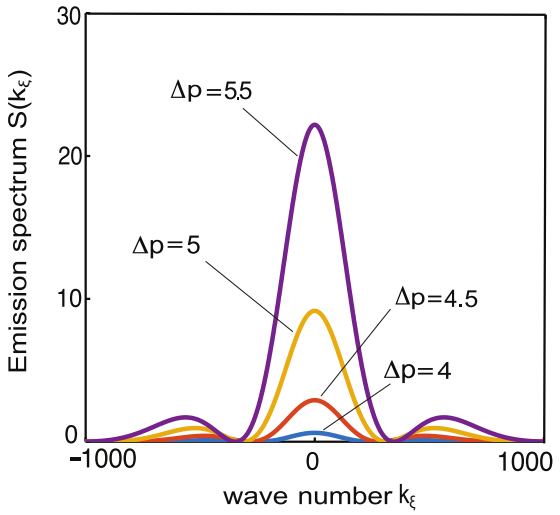

FIG. 1. Emission spectrum according to Eq. (5) at a fixed normalized time $\tau = 1$ versus the wave vector k_ξ in units of κn_0.

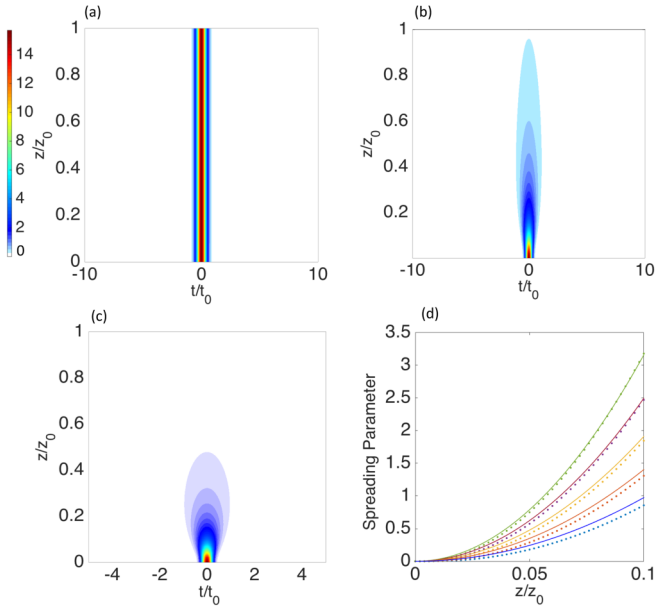

FIG. 2. Square modulus of the quantum-average of the soliton field in linear scale in function of both propagation distance, and time in (a) the classical, and quantum regimes (b) $\Delta p = 2\kappa n_0$, and (c) $\Delta p = 5\kappa n_0$. (d) shows the variance of the quantum soliton with respect to the classical soliton at evenly spaced values of, i.e., $\Delta p =$ 1 (blue) to $\Delta p = 5$ (green) in unit of κn_0. All figures are in units of $z_0 = t_0^2/\beta_2$ and $t_0 = \sqrt{\hbar\omega_0|\beta_2|/\gamma P_{\text{peak}}}$ where P_{peak} is the peak power of the pulse and γ the nonlinearity.

These results establish the connection between the quantum diffusion and the emission. Intuitively one may then view the quantum diffusion as due to a series of emission events from the underlying $N = 1$ soliton, the COM recoiling after each such event. This notion of emission from the underlying soliton is contrary to classical theory in which an energy gap ensures stability [36].

III. STOCHASTIC SIMULATIONS

To further support our analysis, we resort to the numerical solution of the full quantum model. The QNLSE is an operator equation and cannot be directly solved numerically. Phase-space methods map the QNLSE to equivalent stochastic differential equations (SDEs) [37,38]. We use the positive P representation that transforms the Heisenberg equations of motion into a Fokker-Planck equation [35,37,39], which corresponds to a Itô set of differential equation [38]. The quantum field is then represented by a stochastic field, and ensemble averages built from realizations of the stochastic classical field provide the observable quantum averages. The Itô set of differential equation is solved numerically by a fourth-order pseudospectral stochastic Runge-Kutta algorithm. The system is fully quantized and thus results in a stochastic system of differential equations for the pulse propagation. The algorithm used, thus, cannot be a traditional fourth-order Runge-Kutta, but more sophisticated algorithms, that take into account the stochastic nature of the system are needed [40,41]. We first numerically validate the quantum spreading in Eq. (3) by studying the transition from the evolution of the invariant classical soliton to the evaporating quantum soliton. Figure 2 shows the dynamics of the quantum soliton with increasing Δp. $\Delta p = 0$ corresponds to a classical theory and absence of spreading as shown in Fig. 2(a). For $\Delta p > 0$ Figs. 2(b), 2(c) very clearly show the quantum spreading during the nonlinear propagation, the amount of quantum spreading increasing with Δp.

When $\Delta p \ll \kappa$ the center-of-mass of the soliton is localized and the quantum fluctuations are irrelevant [23]. In Fig. 2(d) we show the calculated variance of the stochastic field and find very good agreement between theory and simulations. As the quantum fluctuations are irrelevant in the limit $\Delta p \ll \kappa$ the quantitative comparison with the theory improves when Δp increases.

The sidebands emitted from the evaporating soliton [Figs. 3(a), 3(b)] are composed of frequency-entangled photon pairs. In order to show this, we follow the approach outlined in Ref. [42] but here adapted to ω domain and calculate the second-order correlation function:

$$G^{(2)}(\omega,\omega') = \frac{\langle :n(\omega)n(\omega'): \rangle}{\langle n(\omega)\rangle\langle n(\omega')\rangle} = \frac{\langle a^\dagger(\omega)a^\dagger(\omega')a(\omega)a(\omega')\rangle}{\langle a^\dagger(\omega)a(\omega)\rangle\langle a^\dagger(\omega')a(\omega')\rangle}. \tag{8}$$

From Fig. 3(c) we can observe two areas of clear negative correlation in correspondence of the spectral sidebands that for a scaled propagation length $z/z0 = 0.5$ are located at $\omega/\omega_0 \approx \pm 5$, and are indicated by dashed circles in the figure. There are other regions of negative correlations in the spectrum located at symmetric positions with respect to the central peak. These extra regions presumably correspond to unresolved correlated sidebands that are closer to the center of the pulse, and also regions in proximity of the pulse maximum that are correlated with the central frequency itself. In order to obtain the result shown in Fig. 3(c), we had to perform 10^3 realizations of the pulse propagation, each time with different starting noise. After a large number of realizations the regions with $G^{(2)}(\omega,\omega') - 1 < 0$ emerge in the picture. Thus from

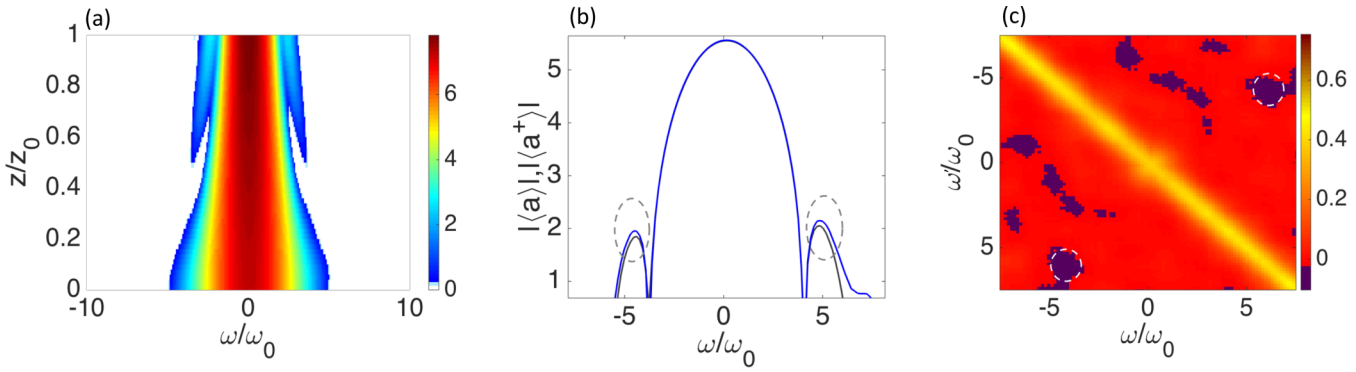

FIG. 3. (a) Evolution in the dimensionless frequency domain in log scale. (b) Average value of $|a(\omega)|$ and $|a^{\dagger}(\omega)|$ for a dimensionless propagation distance $z/z_0 = 0.5$ in logarithmic scale (c) Second order correlation function $G^{(2)}(\omega, \omega') - 1$ for a dimensionless propagation distance $z/z_0 = 0.5$. The dashed ellipses indicate the location of the spectral sidebands seen in (b) and where quantum correlations are also observed in (c).

Fig. 3(c), we can conclude that the emitted sidebands are composed by frequency-entangled photon pairs [42].

IV. REAL-WORLD NUMBERS

Writing Eq. (7) dimensional units, and for the case of solitons in an optical fiber, we obtain for the peak frequency ω_e of the emitted spectrum (corresponding to $k_{\xi}^{(e)}$ in quantum soliton units)

$$\omega_e = \frac{\pi \hbar \omega_0 \beta_1 n_2}{A_{\text{eff}} |\beta_2| n_0 \Delta t_0}, \tag{9}$$

where the effective area A_{eff} is a measure of the area, which a fiber mode effectively covers in the transverse dimension [13]. Therefore, for example a soliton coherent state with $t_0 = 10$ fs width will emit in sidebands shifted by $\omega_e = 10$ GHz.

From the numerical simulations, we estimate the normalized collapse distance z_1/z_0 over which the emission will be observed. We get $z_1/z_0 \approx \kappa n_0/(4\Delta p)$ that, in quantum soliton units, corresponds to $\tau_1 = 1/(n_0 \kappa \Delta p)$, given $z_0 = t_0^2/2\beta_2$ [26]. Considering again a 10 fs pulse with a relatively low photon number (10^4) and a momentum dispersion $\Delta p = 10^2 \text{m}^{-1}$ we get $z_1 = 0.25 z_0 \sim 10^6$ m. The photon number we considered so far requires a high nonlinearity; $n_2 \approx 10^{-18} m^2/W$. For a standard silica fiber the nonlinear refractive index is of the order $10^{-20} m^2/W$, that corresponds to 10^{10} photons for 10 fs soliton coherent state. In this scenario the collapse length z_1 rises up to 10^8 m. As recently shown even greater propagation distances are experimentally possible for solitons in temporal optical cavities [43]. Losses accumulated over the long propagation distances required here could hinder the direct observation of entanglement. However, a more robust measurement would be a heralded photon coincidence measurement [44] that would allow to assess (even in the presence of losses, if sufficient photon counts are accumulated) the nonclassical nature of the soliton evaporation in the form of photon pairs.

V. CONCLUSIONS

In summary, we have provided a model in which both the dynamical equation and the field are quantized: solitons, otherwise classically stable, evaporate into correlated photon pairs. The concurrent processes of quantum evaporation and collapse lead to complete dissipation of the localized soliton state. This evaporation is associated to quantum fluctuations of the center of mass of the quantum soliton. Quantum evaporation has been predicted on the basis of semiclassical models in other systems, the most notable being Hawking radiation from an evaporating black hole and similar physics occurring in BECs with transonic flows. However, our analysis is a radical departure from these effects. Quantum soliton evaporation does not require the existence of a horizon or any specific parameter tuning as in semiclassical optical fiber soliton or BEC evaporation [3,5]. Rather, it is purely the result of the full quantization of the dynamics and the resulting fluctuations in the soliton, leading to photon pair emission that is predicted to be observable even in macroscopic states that can be experimentally tested. We have utilized the fact that the soliton dynamics obey a clearly identifiable quantum evolution equation. Such a luxury is lacking in other, e.g., gravitational systems, but the physics studied here may provide insight and guidance towards fully quantized models in different settings.

ACKNOWLEDGMENTS

We acknowledge discussions with Maria Chiara Braidotti, Giulia Marcucci, and Ewan M. Wright. This publication was made possible through the support of a grant from the John Templeton Foundation (58277). L.D.M.V. acknowledges also support from EPSRC (UK, Grant No. EP/L015110/1) under the auspices of the Scottish Centre for Doctoral Training in Condensed Matter Physics. D.F. acknowledges financial support from the European Research Council under the European Union Seventh Framework Programme (FP/2007-2013)/ERC GA 306559 and EPSRC (UK, Grant No. EP/M009122/1). F.B. acknowledges funding from the German Max Planck Society for the Advancement of Science (MPG) via the IMPP partnership between Scottish Universities and MPG.

APPENDIX A: POSITION AND MOMENTUM QUANTUM FLUCTUATIONS

For quantum optical solitons it is possible to define the mean position operator [22]

$$\hat{\xi} = \left[\int d\xi\, \xi \hat{\phi}^{\dagger}\hat{\phi}\right]\hat{N}^{-1}, \tag{A1}$$

which can be interpreted as the position operator of the center of mass of the photons system. The momentum and position quantum fluctuations are given by [23]

$$\langle \Delta P^2\rangle \approx (n_0 \Delta p)^2 \qquad \text{if } n_0 \gg 1, \tag{A2a}$$

$$\langle \Delta \xi^2\rangle \approx \frac{1}{4\Delta p^2}\frac{1}{n_0^2} + 4(\Delta p)^2\tau^2 \quad \text{if } n_0 \gg 1. \tag{A2b}$$

From these relations we see that when $\Delta p \to 0$ and $n_0 \gg 1$, the momentum and mean position quantum fluctuations vanish, since (A2a) and the time-dependent part of (A2b) go to zero. From (A2b) it is possible to compute the scaled distance of the soliton quantum collapse [29]

$$\tau_1 \simeq \frac{1}{n_0 \kappa \Delta p}, \tag{A3}$$

that diverges in the limit $\Delta p \to 0$.

We now show, reintroducing SI units, with reference to an optical fiber, that the limit $\Delta p \to 0$ corresponds to the classical one. Using the following change of variables:

$$\xi = \beta_1^{-1} t - z,$$
$$\tau = \frac{1}{2}\frac{\beta_2}{\beta_1^2} z, \tag{A4}$$

we obtain

$$\langle \Delta t^2\rangle \approx t_0^2 + 4\Delta p^2 \left(\frac{\beta_2}{\beta_1}\right)^2 z^2, \tag{A5}$$

where we used

$$t_0^2 = \frac{1}{4(n_0\beta_1\Delta p)^2}, \tag{A6}$$

with t_0 initial width of the soliton pulse. From this relation we have

$$\Delta p = \frac{\beta_1}{2 n_0 t_0}, \tag{A7}$$

using $n_0 = \frac{\mathcal{E}}{\hbar\omega_0}$, where ω_0 is the leading frequency of the pulse band and $\mathcal{E}$ the initial energy, we can write

$$\Delta p = \frac{\hbar\omega_0\beta_1}{t_0\mathcal{E}}. \tag{A8}$$

Thus (A5) can be rewritten as follows:

$$\langle \Delta t^2\rangle \approx t_0^2 + 4\left(\frac{\hbar\omega_0}{\Delta t_0 \mathcal{E}}\right)^2 \beta_2^2 z^2. \tag{A9}$$

For $\hbar \to 0$ the time-dependent part of (A9) goes to zero. Thus we proved that the limit $\Delta p \to 0$ corresponds with the classical limit $\hbar \to 0$.

APPENDIX B: CALCULATION OF THE SOLITON SPECTRUM

In this Appendix we derive in detail the soliton spectrum given in Eq. (B11):

$$\langle \hat{a}\rangle_{\psi_s} = \sum_n a_n a_n^* \int dp dp'\, g_n^*(p') g_{n+1}(p)\, \langle n, p', \tau | a | n+1, p, \tau\rangle\,, \tag{B1}$$

we first compute

$$\langle n, p'|\hat{a}|n+1, p\rangle = \int d\xi\, e^{-ik_\xi \xi}\, \langle n, p'|\hat{\phi}(\xi)|n+1, p\rangle$$
$$= C_n\, \mathrm{sech}\left[\frac{\pi}{\kappa}(p-p')\right]\delta[(n+1)p - np' - k_\xi], \tag{B2}$$

where $C_n = \sqrt{n(n+1)}/2|\kappa|^{-1/2}$. We obtained a δ function centered in $k_\xi = (n+1)p - np' \sim n\Delta p = \sqrt{\langle(\Delta P)^2\rangle}$. We can now compute the mean value of the annihilation operator on the state $|\psi_s\rangle$

$$\langle \psi_s|\hat{a}|\psi_s\rangle = \sum_n a_n^* a_{n+1} \int dp dp'\, g_n^*(p') g_{n+1}(p)\, \langle n, p', \tau | a | n+1, p, \tau\rangle$$
$$\approx \sum_n a_n^* a_{n+1} C_n \exp\left[i\frac{c^2 n(n+1)}{4}\tau\right]\int dp dp' g^*(p') g(p) \exp\{-i[(n+1)p - np']\xi_0\} \tag{B3}$$
$$\exp\{-i[(n+1)p^2 - np'^2]\tau\}\delta[(n+1)p - np' - k_\xi]\mathrm{sech}\left[\frac{\pi}{\kappa}(p-p')\right].$$

The integration in dp' gives the following phase-matching condition:

$$p' = \frac{n+1}{n}p - \frac{k_\xi}{n}. \tag{B4}$$

The integral we have to solve is then

$$\langle\psi_s|\hat{a}|\psi_s\rangle \approx \sum_n a_n^* a_{n+1} D_n(\tau) \int dp\, e^{-\left(\frac{p}{\Delta p}\right)^2} e^{-\frac{1}{(\Delta p)^2}\left(\frac{n+1}{n}p-\frac{k_\xi}{n}\right)^2} \exp\{-i[(n+1)p - np']\xi_0\} \exp\left\{-i\left[(n+1)p^2 - n\left(\frac{n+1}{n}p - \frac{k_\xi}{n}\right)^2\right]\tau\right\} \operatorname{sech}\left(\frac{\pi k_\xi}{\kappa n}\right), \tag{B5}$$

where $D_n(\tau) = C_n \exp[i\frac{\kappa^2 n(n+1)}{4}\tau]$. This integral can be evaluated using the stationary phase method. The stationary phase point is given by

$$\frac{d}{dp}\{[(n+1)p - np']x_0 + [(n+1)p^2 - np'^2]\tau\} = 0. \tag{B6}$$

Solving this equation we easily obtain

$$p_0(k_\xi) = k_\xi. \tag{B7}$$

At first order $1/\sqrt{\tau}$ there is no emission peak in the spectrum for $k_\xi \neq 0$. We find spectral peaks at the second order. We remark that one has to take into account a spectral cutoff due to the narrow band of the field around ω_0, as originally outlined in Ref. [35]. The cutoff appears in the upper and lower limits of the integral with respect to p. The second-order $1/\tau$ is computed as follows. Given an integral of the form

$$I = \int_a^b d\xi\, f(\xi) e^{i\tau g(\xi)}, \tag{B8}$$

the solution up to this order is [45]

$$I \approx \frac{1}{\tau}\left[\frac{f(b)}{g'(b)}e^{ig(b)\tau} - \frac{f(a)}{g'(a)}e^{ig(a)\tau}\right]. \tag{B9}$$

Using (B9) and considering $\bar{p} \gg k_\xi$ and $n \gg 1$ the result of the integration is

$$\frac{1}{n\tau}\operatorname{sech}\left[\frac{\pi k_\xi}{\kappa n}\right]\frac{f(k_\xi;\Delta p)}{2\bar{p}}\left[e^{+\frac{2}{(\Delta p)^2}\bar{p}k_\xi/n} e^{-2i\bar{p}k_\xi t} + e^{-\frac{2}{(\Delta p)^2}\bar{p}k_\xi/n} e^{2i\bar{p}k_\xi\tau}\right] \tag{B10}$$

with $f(k_\xi;\Delta p) = e^{-\frac{\bar{p}^2}{\Delta p^2}} e^{-\frac{k_\xi^2}{(n\Delta p)^2}}$.

Considering $n \approx n_0$ with n_0 average photon number we can drop the summation on n in (B5) and compute the square modulus

$$S(k_\xi,\tau) = |\langle\psi_s|\hat{a}|\psi_s\rangle|^2 \approx \frac{1}{n_0^2\tau^2}\operatorname{sech}^2\left(\frac{\pi k_\xi}{\kappa n_0}\right)\frac{f^2(k_\xi;\Delta p)}{2\bar{p}^2}\left[\cosh\left(\frac{2}{\Delta p^2}\frac{k_\xi}{n_0}\bar{p}\right) + \cos(\bar{p}k_\xi\tau)\right]. \tag{B11}$$

From (B11) it is possible to compute the relation between the emission wave numbers k_ξ and Δp. We use the following approximation:

$$n_0 \gg n_0\kappa \gg 1, \tag{B12}$$

and the scale of the soliton collapse, i.e., $\tau_1 = \frac{1}{n_0\kappa\Delta p}$ [29,30]. Within this approximation (B11) becomes

$$S(k_\xi,\tau_1) \approx \frac{2}{n_0^2\tau^2}\operatorname{sech}^2\left(\frac{\pi k_\xi}{n_0\kappa}\right)\left[1 + \cos\left(\frac{\bar{p}k_\xi}{n_0\kappa\Delta p}\right)\right]. \tag{B13}$$

Considering the spectrum for $k_\xi \gg 1$ with the approximations (B12) we get

$$S(k_\xi,\tau_1) \approx e^{-\frac{2\pi k_\xi}{n_0\kappa}}\left[2 + \cos\left(\frac{\bar{p}}{n_0\kappa\Delta p}k_\xi\right)\right]. \tag{B14}$$

It is easy to show that the maxima of this spectrum are

$$k_\xi^e = \pm(2n+1)\pi n_0\kappa\frac{\Delta p}{\bar{p}} \quad n \in \mathbf{Z}. \tag{B15}$$

It is now interesting to write (B15) in terms of relevant physical quantities; with reference to fiber optics we rewrite the emission wave number

$$k_\xi^{(e)} = \pi n_0\kappa\frac{\hbar c\beta_1}{\mathcal{E}\Delta t_0} = \hbar\pi c\frac{\beta_1^2}{|\beta_2|}\frac{\gamma}{n_0\Delta t_0}, \tag{B16}$$

where we have used $\Delta p = \frac{\beta_1\hbar\omega_0}{\mathcal{E}\Delta t_0}$ as we computed in the previous section and the definition of the cutoff $\bar{p} = \frac{\omega_0}{c}$ [35]. In term of a frequency (B16) become

$$\omega^{(e)} = \beta_1^{-1}k_\xi^{(e)} = \frac{\hbar\beta_1\omega_0\pi n_2}{A_{\text{eff}}|\beta_2|n_0\Delta t_0}, \tag{B17}$$

where we used $\gamma = n_2\omega_0/cA_{\rm eff}$, with $A_{\rm eff}$ the effective area of the fiber.

APPENDIX C: MINIMAL INTRODUCTION TO PHASE-SPACE METHODS

The QNLSE is an operator equation and it can not be directly solved with numerical approaches. It is thus necessary to use phase-space methods [39], which map operator equations to equivalent stochastic differential equation (SDEs). We use the positive P representation; it transforms the Heisenberg equations of motion to a Fokker-Plank (FP) equation [35,37]. The functional P representation is defined, in a $2N$-dimensional phase space, by

$$\hat{\rho}(t) = \int D\mu[\boldsymbol{\alpha},\boldsymbol{\beta}]P[\boldsymbol{\alpha},\boldsymbol{\beta}]\hat{\lambda}(\boldsymbol{\alpha},\boldsymbol{\beta}). \tag{C1}$$

The kernel $\hat{\lambda}(\boldsymbol{\alpha},\boldsymbol{\beta})$ is a projection operator onto an off-diagonal pair of coherent states $|\boldsymbol{\alpha}\rangle$, $|\boldsymbol{\beta}\rangle$:

$$\hat{\lambda}(\boldsymbol{\alpha},\boldsymbol{\beta}) = \frac{|\boldsymbol{\alpha}\rangle\langle\boldsymbol{\beta}^*|}{\langle\boldsymbol{\beta}^*|\boldsymbol{\alpha}\rangle}. \tag{C2}$$

The positive P representation is defined by choosing the integration measure as a volume measure in the $2N$-dimensional phase space

$$D\mu[\boldsymbol{\alpha},\boldsymbol{\beta}] = \Pi_l d\alpha_l d\beta_l. \tag{C3}$$

The positive nature of $P(\boldsymbol{\alpha},\boldsymbol{\beta})$ means that, whenever the corresponding evolution equation is of the FP type, than an equivalent set of Itô stochastic differential equations exists and describes the motion of the coordinate $(\boldsymbol{\alpha},\boldsymbol{\beta})$ of a fictitious particle in the phase space [37].

Substituting (C1) in the equation

$$i\hbar\frac{d}{dt}\hat{\rho} = [\hat{H},\hat{\rho}] \tag{C4}$$

with $\hat{H}$ given by

$$\hat{H} = \int dx\,(\hat{\phi}_x^\dagger\hat{\phi}_x + \hat{\phi}^\dagger\hat{\phi}\hat{\phi}^\dagger\hat{\phi}). \tag{C5}$$

Writing the Hamiltonian in SI units we get

$$i\hbar\int D\mu\,\hat{\lambda}\frac{\partial}{\partial t}P[\boldsymbol{\alpha},\boldsymbol{\beta}] = \int D\mu\,P[\boldsymbol{\alpha},\boldsymbol{\beta}][H,\hat{\lambda}], \tag{C6}$$

integrating by parts we obtain a Fokker-Plank equation that corresponds to the following Itô set of stochastic equations:

$$\begin{aligned}\alpha_t(x,t) &= -i\frac{\omega''}{2}\alpha_{xx} + i\tilde{\gamma}\alpha^2\beta + \sqrt{(i\tilde{\gamma})}\alpha\xi^{(1)}(x,t),\\ \beta_t(x,t) &= i\frac{\omega''}{2}\beta_{xx} + i\tilde{\gamma}\beta^2\alpha + \sqrt{(-i\tilde{\gamma})}\beta\xi^{(2)}(x,t),\end{aligned} \tag{C7}$$

with $\tilde{\gamma} = \hbar\omega\gamma$. $\xi^(j)$ are time-distance dependent, but mutually independent, real Gaussian white noises. We numerically integrated Eq. (C7) by using a stochastic Runge-Kutta algorithm [41].

APPENDIX D: INITIAL CONDITION FOR THE NUMERICAL SIMULATION

To compute the initial condition for the stochastic numerical simulation we can observe that the initial quantum soliton state $|\psi_s\rangle$ is maximally overlapped with the soliton coherent state [29]. We can realize that by looking at the soliton state at $\tau = 0$

$$|\psi_s,\tau=0\rangle = \sum_{n=0}^{\infty} a_n C_n \int d^n\xi\;\tilde{g}_n(Y_n) \times e^{-|\kappa|/2\sum\limits_{1\leqslant j\leqslant k\leqslant n}|\xi_j-\xi_k|}\frac{1}{n!}\prod_{j=1}^{n}\hat{\phi}^\dagger(\xi_j)\,|0\rangle\,, \tag{D1}$$

with a_n a Poisson distribution of the photon number, $C_n = \sqrt{(n-1)!/2\pi\,|\kappa|^{n-1}}$ and $\tilde{g}_n(Y_n)$ the Fourier transform of the Gaussian superposition of momenta with $Y_n = \sum_{j=1}^{n}\xi_n$. This is a coherent superposition of eigenstates of the QNLS Hamiltonian, and, even if this state is more complicated than a simple soliton coherent state, the case of large mean photon numbers, a condition easily met experimentally, exhibits closest-to-classical behaviors like an ordinary coherent state [29]. To prove that this state is maximally overlapped with a pulse coherent state one could compute explicitly the overlap amplitude and observe that has a maximum at $\tau = 0$ [29]. A less rigorous, but simpler way to prove this result is to look at the expectation value of the quantum field $\hat{\phi}(x,t)$ always at $\tau = 0$. For a large photon number n_0 we get

$$\langle\psi_s,\tau|\hat{\phi}(\xi)|\psi_s,\tau\rangle\,|_{\tau=0} \approx n_0\frac{\kappa}{2}\,\mathrm{sech}\left(\frac{n_0}{2}\kappa\xi\right)e^{-(\Delta p\xi)^2}, \tag{D2}$$

which corresponds exactly to the expectation value of a coherent soliton state when $\Delta p = 0$. With this in mind we can now use Eq. (D2) as the initial condition for the numerical simulation, provided that the quantum dynamics is fully mapped into the stochastic dynamics. In the dimensionless units used in the simulation we have

$$\alpha(z/z_0 = 0, t/t_0) = 2\,\mathrm{sech}\left(2\frac{t}{t_0}\right)e^{-\Delta^2\left(\frac{t}{t_0}\right)^2}, \tag{D3}$$

where z_0, t_0 are the normalization scales defined in Fig. (2) and Δ is the scaled momentum fluctuation defined as follows:

$$\Delta = \frac{\Delta p}{\kappa n_0} = \Delta p\sqrt{\frac{|\beta_2|}{\beta_1^2\gamma P_{\rm peak}}}. \tag{D4}$$

with $P_{\rm peak}$ being the peak power of the initial pulse.

[1] M. J. Baird, F. R. Hope, and A. F. G. Wyatt, Nature (London) **304**, 325 (1983).

[2] F. R. Hope, M. J. Baird, and A. F. G. Wyatt, Phys. Rev. Lett. **52**, 1528 (1984).

[3] T. G. Philbin, C. Kuklewicz, S.Robertson, S. Hill, F. König, and U. Leonhardt, Science **319**, 1367 (2008).

[4] S. W. Hawking, Nature (London) **248**, 30 (1974).

[5] J. Dziarmaga, Phys. Rev. A **70**, 063616 (2004).

[6] M. I. Shaukat, E. V. Castro, and H. Terças, Phys. Rev. A **95**, 053618 (2017).
[7] J. Steinhauer, Nat. Phys. **10**, 864 (2014).
[8] J. Steinhauer, Nat. Phys. **12**, 959 (2016).
[9] K. Eppley and E. Hannah, Found. Phys. **7**, 51 (1977).
[10] S. Carlip, Class. Quant. Grav. **25**, 154010 (2008).
[11] P. G. Drazin and R. S. Johnson, *Solitons: An Introduction*, Cambridge Texts in Applied Mathematics (Cambridge University Press, Cambridge, 1989).
[12] V. E. Zakharov and A. B. Shabat, Zh. Eksp. Teor. Fiz. **61**, 118 (1972) [Sov. Phys. JETP **34**, 62 (1972)].
[13] G. P. Agrawal, *Nonlinear Fiber Optics* (Academic Press, New York, 2007).
[14] Y. S. Kivshar and G. Agrawal, *Optical Solitons: From Fibers to Photonic Crystals* (Academic Press, New York, 2003).
[15] C. Becker, S. Stellmer, P. Soltan-Panahi, S. Dorscher, M. Baumert, E.-M. Richter, J. Kronjager, K. Bongs, and K. Sengstock, Nat. Phys. **4**, 496 (2008).
[16] C. S. Gardner, J. M. Greene, M. D. Kruskal, and R. M. Miura, Phys. Rev. Lett. **19**, 1095 (1967).
[17] S. Takeno and S. Homma, Prog. Theor. Phys. **70** (1983).
[18] T. C. Bertrand, M. Alidou, and K. T. Crepin, *Solitons in DNA and Biological Implications* (Scholars' Press, Riga, 2014).
[19] G.-fa Zhou and C.-T. Zhang, Phys. Scr. **43**, 347 (1991).
[20] M. J. Potasek and B. Yurke, Phys. Rev. A **35**, 3974 (1987).
[21] M. J. Potasek and B. Yurke, Phys. Rev. A **38**, 1335 (1988).
[22] Y. Lai and H. A. Haus, Phys. Rev. A **40**, 844 (1989).
[23] Y. Lai and H. A. Haus, Phys. Rev. A **40**, 854 (1989).
[24] G. J. Milburn, Phys. Rev. A **33**, 674 (1986).
[25] D. Yao, Phys. Rev. A **55**, 701 (1997).
[26] E. M. Wright, Phys. Rev. A **43**, 3836 (1991).
[27] E. M. Wright, D. F. Walls, and J. C. Garrison, Phys. Rev. Lett. **77**, 2158 (1996).
[28] M. Greiner, O. Mandel, T. Hänsch, and I. Bloch, Nature (London) **419**, 51 (2002).
[29] D. Yao, Phys. Rev. A **52**, 1574 (1995).
[30] I. G. Gochev and V. J. Draganova, Phys. Rev. A **49**, 5139 (1994).
[31] G. J. Milburn and C. A. Holmes, Phys. Rev. Lett. **56**, 2237 (1986).
[32] R. G. McDonald and A. S. Bradley, Phys. Rev. A **93**, 063604 (2016).
[33] D. B. Creamer, H. B. Thacker, and D. Wilkinson, Phys. Rev. D **21**, 1523 (1980).
[34] W. H. Zurek, S. Habib, and J. P. Paz, Phys. Rev. Lett. **70**, 1187 (1993).
[35] P. Drummond and M. Hillery, *The Quantum Theory of Nonlinear Optics* (Cambridge University Press, Cambridge, 2013).
[36] R. Kanamoto, H. Saito, and M. Ueda, Phys. Rev. A **73**, 033611 (2006).
[37] C. Gardiner and P. Zoller, *Quantum Noise* (Springer, Berlin, 2000).
[38] C. Gardiner, *Handbook of Stochastic Methods*, 4th ed. (Springer, Berlin, 2009)
[39] R. J. Glauber, Phys. Rev. **131**, 2766 (1963).
[40] N. J. Kasdin, Proc. IEEE **83**, 802 (1995).
[41] J. Kasdin, J. Guid. Control. Dyn. **18**, 114 (1995).
[42] I. Carusotto, S. Fagnocchi, A. Recati, R. Balbinot, and A. Fabbri, New J. Phys. **10**, 103001 (2008).
[43] K. Jang, M. Erkintalo, S. G. Murdoch, and S. Coen, Nat. Photon. **7**, 657 (2013).
[44] E. Bocquillon, C. Couteau, M. Razavi, R. Laflamme, and G. Weihs, Phys. Rev. A **79**, 035801 (2009).
[45] F. Olver, *Asymptotics and Special Functions* (Academic Press, New York, 1974).